Self-organized criticality from separator reconnection in solar flares

D. W. Longcope and E. J. Noonan
Department of Physics, Montana State University,
Bozeman, MT 59717

Received ______________________; accepted ______________________

Submitted to Astrophysical Journal

ABSTRACT

A new cellular automaton model for solar flares is presented, in which a complex coronal magnetic field is stressed by photospheric shear. The minimum current corona model is used to describe the slow build-up and sudden release of stress in the field. Stress takes the form of currents flowing along the field's network of magnetic separators; it is released by magnetic reconnection. By this model we show how magnetic reconnection can occur as an avalanche, releasing stress along an extended region of the separator network. The model exhibits self-organized criticality, thus the sizes of reconnection avalanches are distributed with a power-law. Flare durations and peak emission levels are also distributed according to power-laws, with different exponents. Because the model is derived from the application magnetohydrodynamics to a coronal field, it is possible to assign physical sizes to its avalanches. These agree well with the sizes and frequencies of observed flares. The total power from flares of all sizes agrees with observation and is therefore well below the inferred coronal heating power.

1. Introduction

Solar flares are caused by the rapid release of magnetic energy in the solar corona (Gold & Hoyle 1960). Extremely large flares, some releasing as much as 10^{34} ergs (Kane et al. 1995), occur only rarely (perhaps only once per 11 year solar cycle), while smaller flares occur more frequently. Observations have shown that flares of a given size occur at a frequency which is an inverse power of that size

(Lin, Schwartz, & Kane 1984, Dennis 1985). This may be expressed as a power-law relationship with the flare's energy

$$\frac{dN}{dE} \sim E^{-\alpha_E} \quad , \tag{1}$$

where similar powers $\alpha_E \simeq 1.6$ have been measured by several investigators (Crosby, Aschwanden, & Dennis 1993, Bromund, McTiernan, & Kane 1995) using different instruments, over different ranges of energy, and different methods of calculating total flare energy.

1.1. Self-organized criticality

Power-law frequency distributions, with similar exponents, occur in a wide variety of natural systems including earthquakes (Carlson & Langer 1989) and avalanches in a pile of sand (Held et al. 1990). A unified model, called self-organized criticality (SOC), has been proposed to explain this apparently universal behavior (Bak, Tang, & Wiesenfeld 1988). In analogy with the theory of critical phenomena, SOC seems to apply to a diverse set of phenomena due to a universal feature of interacting sub-systems (Kadanoff et al. 1989). Thus while the detailed physics in earthquakes, avalanches and solar flares seem utterly different, each may be considered as a large-scale manifestation of small interacting elements. In each case there seem to be many small-scale "failures" which trigger each other to produce a single large-scale event. For example, a single grain of sand added to a pile at its angle of repose may slide downhill. This could be viewed as a very small avalanche (one grain of sand), however, it is possible for this single grain to dislodge other grains, thereby causing a larger avalanche. According to the SOC theory, the distribution of avalanche sizes depends not on the physics of the individual grains, but on the fact that they interact. If solar flares are also caused by the interaction of small-scale failures, then it would be natural that their distribution be a power-law as well.

Self-organized criticality of interacting sub-systems is often studied using cellular automaton (CA) models. A CA model consists of a spatial lattice of individual elements. Each element evolves according to a simple set of *rules*, which include an interaction between neighboring elements. A simple CA model which exhibits SOC was developed by Bak, Tang and Weissenfeld (1988); they called the model a *sandpile*. Avalanches in the sandpile model are distributed according to a power-law whose exponent depends on the dimensionality of the lattice and the universality class to which the rules belong (Kadanoff et al. 1989). In particular, modifications to the rules which obey basic conservation laws (i.e. conservation of energy) will not change the universality class, and therefore they will not change the exponent. Two dimensional sandpile models exhibit powers $\alpha \simeq 1.05$, while three dimensional models exhibit $\alpha \simeq 1.5$ (Bak, Tang, & Wiesenfeld 1988, Kadanoff et al. 1989).

A CA model for solar flares, fundamentally similar to the sandpile, was first proposed by Lu and Hamilton (1991), and several different CA models for solar flares have been proposed since then (Zirker & Cleveland 1993, Vlahos et al. 1995, MacKinnon & Macpherson 1997, Vassiliadis et al. 1998, Chou 1999). While different in several respects, these models have features in common with each other and the Lu and Hamilton (LH) model. Because of these common features most of the following discussion will refer to the LH model. The LH model consists of elements representing magnetic field vectors, arranged in a three-dimensional cubic lattice. Randomly selected elements are changed until one element differs from its neighbors by more than a set amount (threshold). The differing element is 'relaxed" by changing its value and, by a smaller amount, the values of its neighbors. These changes can cause nearby elements to differ from *their* neighbors, necessitating other relaxation episodes. An extended avalanche of magnetic relaxation may result, representing a large flare.

The size, E, of an avalanche is the number of individual relaxation episodes it involves. This quantity is distributed with a power-law whose exponent is $\alpha_E \sim 1.51$ (Lu & Hamilton 1991), the same as that in the 3-dimensional sandpile of Bak, Tang and Weisenfeld. An avalanche can also be characterized by its duration, D, and peak relaxation rate, P, which are distributed with exponents $\alpha_D \simeq 1.88$ and $\alpha_P \simeq 1.86$ respectively (Lu et al. 1993).

This simple model agrees well with observational data from solar flares. For example, X-ray data from ISEE-3 show solar flares as short pulses in the full-disk light-curve. The integrated flux (fluence), peak count-rate and duration of these pulses each have power-law distributions whose exponents are very similar to those from the corresponding quantity in the LH model (Bromund, McTiernan, & Kane 1995).

While it seems to match the observed distributions well, there are several limitations in the LH model. A self-consistent three-dimensional CA model can represent the solar magnetic field only on extremely small scales. The coronal field strength decreases with height with typical dimension $\sim 10^9$ cm. Since the model's three-dimensional lattice is uniform in all directions, including vertically, it must represent scales smaller than 10^9 cm, while the individual elements must represent scales much smaller still. If this were the case it is not clear how the LH model could be applied to the full range of solar flare energies, since many of the larger flares span horizontal distances of 10^9 cm or more.

While the rules of the LH model resemble a kind of magnetic relaxation, they cannot be derived from basic dynamical equations such as magnetohydrodynamics (MHD). This fact contributes to the difficulty assigning a physical scale to the elements in the model. One notable exception is the two-dimensional sandpile-like CA model of Zirker and Cleveland (1993), which exhibits a power-law $\alpha_E \simeq 1.0$. Recently Vassiliadis et al. derived a related CA model from a magnetic diffusion equation whose diffusivity was applied only intermittently. Moreover, no CA model yet proposed has used elementary rules of the kind successfully applied to the analysis of an observed solar flare. This fact makes it difficult to use any such model to make quantitative studies.

1.2. Separator reconnection

It is a common view that coronal activity, such as flaring, results from the magnetic interaction between isolated photospheric sources (Sweet 1958, Gold & Hoyle 1960). The Minimum Current Corona (MCC; Longcope 1996) model is a quantitative model for the buildup of coronal currents as photospheric sources move relative to one another. It is a quasi-static MHD model in which all coronal current is confined to topological interfaces called *separators*. The MCC employs a simplified model called *stick-slip* reconnection to describe the occasional release of stress at the separators. Applied to magnetograms of the active region complex AR6993/6994 the MCC successfully predicted the location, morphology and energy of a flare on Jan 7, 1992 (Longcope & Silva 1998). It has also been used to study impulsive brightenings in an X-ray bright point found in TRACE observations (Kankelborg & Longcope 2000).

Coronal currents in the MCC interact with one another through mutual inductance, making it possible for one reconnection episode to trigger another nearby. This kind of sympathetic flaring was predicted and observed in flare Jan. 7, 1992, where the field included a complex of twelve separators. A truly complicated magnetic field might actually contain hundreds or thousands of separators (Welsch & Longcope 1999), all interacting with one another through mutual inductance. This suggests that reconnection in a complex magnetic field could occur in avalanches of propagating episodes, perhaps creating a self-organized critical state. The present work shows this to be the case; the MCC reconnection model, when applied to certain complex coronal fields, exhibits SOC. The distribution of flare sizes is therefore a power-law. As in previous studies this fact is here demonstrated by developing a CA model. Rules for this new CA model, to be called the MCC/CA, will be derived directly from the MCC model, which follows in turn from equations of MHD (Longcope 1996).

The MCC/CA model derived below differs from previous models, discussed above, in several fundamental ways. The model is set on a two-dimensional lattice, representing the solar surface, in contrast to the uniform three-dimensional lattices of previous models. Individual elements of the lattice are magnetic separators whose physical sizes and distribution are determined by the photospheric flux. For this reason the new model, unlike previous ones, has a well-defined physical scale, and a geometry with clear connection to the corona. Secondly, the model is driven externally by a steady motion (a shearing) of the photospheric flux, and obeys completely deterministic rules, in contrast to previous models whose rules invoked some random component. The exponent governing the energy distribution, $\alpha_{_E} = 1.34 \pm 0.05$, differs from that of a two-dimensional sandpile model, and presumably from a two-dimensional LH model.

This work presents a full derivation of the MCC/CA, a demonstration that it exhibits SOC and a quantitative comparison of its predictions to observations. The next section reviews the general MCC model for reconnection at one or more separators. Section 3 applies the MCC to a square lattice of photospheric sources subject to a shearing motion. The continuous dynamical evolution of this system is then approximated by a discrete set of steps; this is the CA model. The CA model is implemented in §4, yielding a frequency distribution of avalanche sizes, durations and peak emission rates. Coronal parameters are then applied to the model results, in §5, to predict sizes and frequencies of solar flares. These predictions compare favorably to solar flares. Finally, in §6 we discuss the possible limitations of our model, and how we expect it to apply to more realistic geometries.

2. Separator reconnection in solar flares

2.1. The minimum current corona model

To understand the MCC, consider a bipole composed of two photospheric sources, P and N, with opposite signs and equal fluxes. Assume that the sources share magnetic flux with one another (see fig. 1a) as well as other more distant sources (not shown). That flux shared between P and N is separated from other field by a single magnetic field line called a *separator* (Greene 1988, Lau & Finn

1991, Longcope 1996) and labeled σ in fig. 1a. The total amount of shared flux Φ_σ can be calculated as

$$\Phi_\sigma \;=\; \int_S \mathbf{B}\cdot d\mathbf{A} \quad , \tag{2}$$

using a surface S whose perimeter consists of σ above and $z = 0$ below. In a current-free corona (a vacuum), the shared flux $\Phi_\sigma^{(\mathrm{v})}$, will depend on the locations of *all* photospheric sources. Motions of the sources will generate coronal currents so $\Phi_\sigma \neq \Phi_\sigma^{(\mathrm{v})}$ in general.

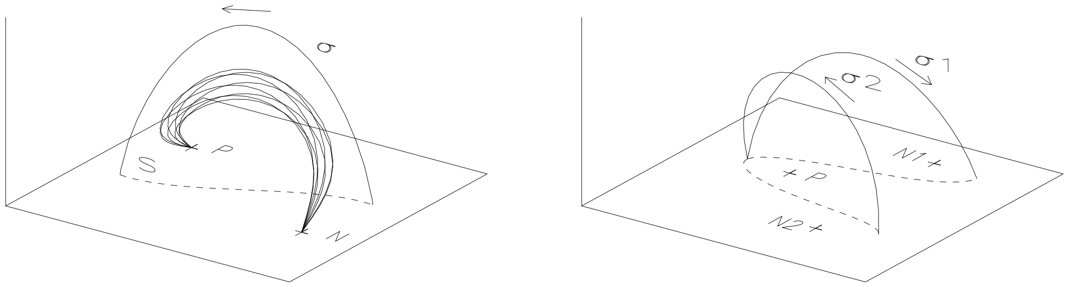

Fig. 1.—. Field lines in simple source configurations. (a) Field lines from the bipole P/N with the single separator σ. (b) Three sources, with two separators σ_1 and σ_2. Separator currents flowing in the indicated directions will contribute self-flux with the same sense as the vacuum flux; the mutual inductance $M_{12} < 0$ will be negative.

In the ideal MHD equilibrium currents flow only in singular ribbons along separators (Longcope & Cowley 1996). Current I_σ flowing along the separator σ will give rise to a self-flux $\Phi_\sigma^{(\mathrm{cr})} = \mathcal{L}_\sigma I_\sigma$, where $\mathcal{L}_\sigma$ is the self-inductance of the separator (cgs-emu units are used throughout). Ignoring, for the moment, any contributions from other coronal currents, the total shared flux

$$\Phi_\sigma \;=\; \Phi_\sigma^{(\mathrm{v})} \;+\; \mathcal{L}_\sigma\, I_\sigma \tag{3}$$

combines the vacuum and the self-flux contribution.

Prescribed motion of the sources will change the vacuum flux $\Phi_\sigma^{(\mathrm{v})}$ in a prescribed way. In MCC separators are modeled as conductors with two distinct states analogous to a household fuse. In its *normal* state the separator is a perfect conductor which, by Faraday's law, forbids flux change: $\dot{\Phi}_\sigma = 0$. Assuming that the self-inductance is unaffected by the source motion eq. (3) requires that the current change by

$$\Delta I_\sigma \;=\; -\,\mathcal{L}_\sigma^{-1}\,\Delta\Phi_\sigma^{(\mathrm{v})} \quad , \tag{4}$$

for a change $\Delta\Phi_\sigma^{(\mathrm{v})}$ in vacuum flux. For example, as poles P and N approach they "seek" to share more flux; $\Phi_\sigma^{(\mathrm{v})}$ increases so $\Delta\Phi^{(\mathrm{v})} > 0$. According to eq. (4) the separator, in its normal state, will experience a change in current $\Delta I_\sigma < 0$ flowing against the arrow in figure 1a. This sense of current will create a self-flux directed toward P thereby cancelling the change in vacuum flux.

In its other state, called *reconnective*, the separator's conductivity is dramatically reduced and Φ_σ does change. The separator enters this state when, during the course of normal-state evolution, its current is driven above a threshold $|I_\sigma| \ge I^\star$. This simple model, analogous to an electrical fuse, is called stick-slip reconnection (Longcope 1996). The normal/reconnective transition is intended to represent the triggering of some unspecified plasma instability which enhances the plasma resistivity in the vicinity of the current sheet. The lowered conductivity yields a loop voltage around σ causing $\Phi_\sigma \to \Phi_\sigma^{(\mathrm{v})}$ and $I_\sigma \to 0$. This is called a "reconnection episode" and it lasts only a few Alfvén transit times. At the end of the reconnection episode $I_\sigma = 0$ and the separator returns to its normal state.

2.2. Mutual inductance

In more complicated magnetic fields there are several separators whose currents may interact. Consider the case with three poles and two separators depicted in fig.1b. The fluxes through separators σ_1 and σ_2 include vacuum flux and self-flux contributions as well as new mutual inductance terms

$$\Phi_1 \;=\; \Phi_1^{(\mathrm{v})} \;+\; \mathcal{L}_1\, I_1 \;+\; M_{12}\, I_2 \quad , \tag{5}$$

$$\Phi_2 \;=\; \Phi_2^{(\mathrm{v})} \;+\; \mathcal{L}_2\, I_2 \;+\; M_{21}\, I_1 \quad , \tag{6}$$

where $M_{12} = M_{21}$ is the mutual inductance between separators σ_1 and σ_2. For simplicity we will introduce a square symmetric matrix M_{ij} whose off-diagonal elements are mutual inductances and whose diagonal elements $M_{ii} = \mathcal{L}_i$ are the self-inductances. The flux relationships, (5) and (6), are then

$$\Phi_i \;=\; \Phi_i^{(\mathrm{v})} \;+\; \sum_j M_{ij}\, I_j \quad , \tag{7}$$

for both $i = 1$ and $i = 2$.

While both separators are in their normal states their fluxes Φ_i do not change, even as their vacuum fluxes $\Phi_i^{(\mathrm{v})}$ do. In this case the currents in each separator will change

$$\dot{I}_i \;=\; -\sum_j [M^{-1}]_{ij}\, \dot{\Phi}_j^{(\mathrm{v})} \quad , \tag{8}$$

where M^{-1} is the inverse of the matrix M. This is the *stressing phase* of evolution, it lasts until one of the separators reaches the threshold $|I_i| = I^{\star}$. If separator 1 crosses the threshold first, then the stressing phase ends as it transitions into its reconnective state. Its flux then changes so as to take $I_1 \to 0$. Due to the contribution from I_2, however, this is not equivalent to $\Phi_1 \to \Phi_1^{(\mathrm{v})}$.

While separator 1 undergoes a reconnection episode separator 2 remains in its normal state so Φ_2 stays fixed. Furthermore, the reconnection episode is short compared to the stressing phase so neither vacuum flux will change. In order to hold both Φ_2 and $\Phi_2^{(\mathrm{v})}$ fixed while I_1 changes it is necessary that I_2 also change. From (6) we have

$$\Delta I_2 \;=\; -\,\mathcal{L}_2^{-1}\,M_{21}\,\Delta I_1 \quad . \tag{9}$$

In this way a reconnection episode on separator 1 changes the current on separator 2. Since $M_{12} < 0$ in fig. 1b, both currents will change in the same sense relative to their respective arrows.

Prior to the reconnection episode in separator 1, $|I_2| < I^{\star}$ (otherwise the stressing phase would have ended with separator 2 reconnecting.) The subsequent change in I_2, eq. (9), might take separator 2 across the threshold. If this were to happen then separator 2 would enter the reconnective state and $I_2 \to 0$. This is a *sympathetic* reconnection episode triggered by reconnection on separator 1. The communication between separators travels at the Alfvén speed, about the same time each individual episode lasts. It is therefore likely that the consequences of their energy release, e.g. X-ray emission, will appear as a single elongated event: a *flare*. For bookkeeping simplicity, however, we will assume the first episode is complete, and separator 1 has returned to is normal state, before initiating the second. For this reason I_1 will have changed from zero as a result of the second episode.

The relaxed state will always have less magnetic energy than the pre-reconnection state. This difference in magnetic energies is assumed to cause the effects associated with flares, such as radiation and particle acceleration. The difference in energy can be calculated by integrating the electromagnetic work which would be generated if the flux Φ_i were changed quasi-statically

$$\frac{dW}{dt} \;=\; I_i\,\frac{d\Phi_i}{dt} \;=\; I_i\,\mathcal{L}_i^{(\mathrm{eff})}\,\frac{dI_i}{dt} \quad . \tag{10}$$

The effective self-inductance $\mathcal{L}_i^{(\mathrm{eff})}$ accounts for the effects of all other currents which change as a result of a change in I_i, thereby effecting Φ_i. Note that $\dot{\Phi} = 0$ on all separators except the one reconnecting, so there are no other contributions to the total magnetic energy. Ignoring a time variation in $\mathcal{L}_i^{(\mathrm{eff})}$ the energy released by a relaxation episode taking $I_i \to 0$ from the threshold is

$$\Delta E \ = \ \tfrac{1}{2}\mathcal{L}_i^{(\mathrm{eff})}\,(I^\star)^2 \quad . \tag{11}$$

This is positive as long as $\mathcal{L}_i^{(\mathrm{eff})} > 0$. Thus the initial relaxation of separator σ_1 releases an energy proportional to $\mathcal{L}_1^{(\mathrm{eff})}$, and the sympathetic relaxation of σ_2 releases energy proportional to $\mathcal{L}_2^{(\mathrm{eff})}$.

The discussion above indicates how energy storage and release is treated by the MCC model as distinct reconnection episodes. Moreover, we have shown how one episode can trigger another in a neighboring separator. A truly complex magnetic field will contain a large network of separators in which it seems possible for a single reconnection episode to trigger a large number of others in a kind of avalanche. We propose that this is a natural state of affairs in a complex separator network, and furthermore, that this kind of "avalanche" behavior leads naturally to a universal distribution of event sizes.

3. The cellular automaton model

To explore the propagation of reconnection episodes in a network of separators we present an approximation of the MCC in the form of a cellular automaton (CA). For this purpose we consider a square network of separators arising from a regular lattice of equal sources. The sources are arranged in a $N \times N$ square lattice with lattice constant L. Signs alternate in a checkerboard pattern as shown in fig. 2. At each edge lies a single separator enclosing the flux shared between the charges in the adjacent cells.

The model will track the currents I_i in each of the separators, through a sequence of steps $I_i^n \to I_i^{n+1}$. Each step will consist of a stressing phase followed by a reconnection phase. By convention positive I_i will represent rightward or upward current, and will be rescaled to the threshold $I^\star$. To match this convention we define vacuum flux $\Phi_i^{(\mathrm{v})}$ to be positive if it is directed upward or leftward.

The model will consider the evolution induced by a shearing of the sources as shown in fig. 2. This shearing will increase the separation between vertical neighbors causing the magnitude of $\Phi_i^{(\mathrm{v})}$ to decrease for horizontal separators. Sharing less (unsigned) flux with vertical neighbors a source will share *more* flux with its horizontal neighbors. Therefore the magnitude of $\Phi_i^{(\mathrm{v})}$ will increase on vertical separators exactly as quickly as it decreases on horizontal separators. Defining a

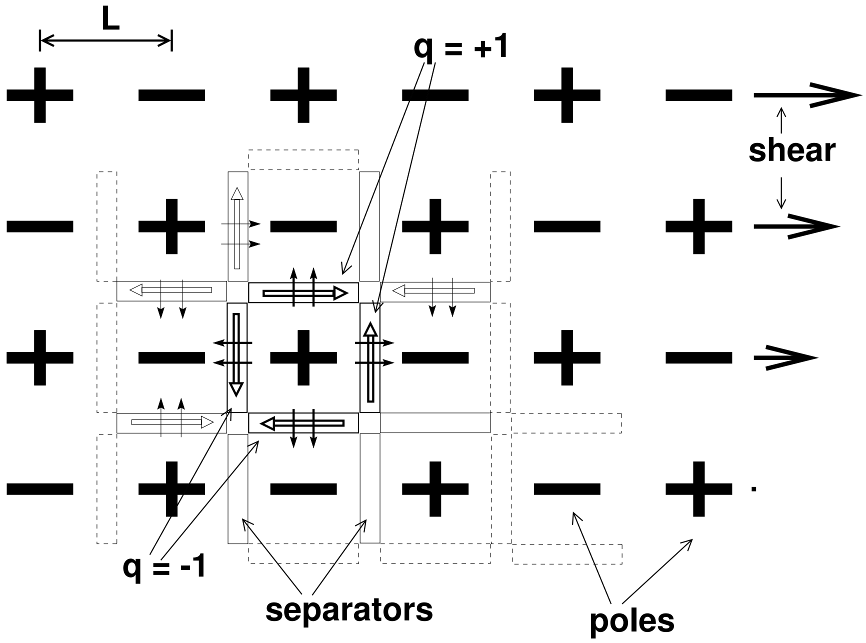

Fig. 2.—. The geometry of the model. Poles, labeled + and −, are arranged in a square lattice. Separators lie along edges. The direction of the vacuum field is shown by thin arrows. The change in this flux, due to shearing, defines a value $q_i = \pm 1$ at each separator. Current flowing in the q_i direction, as created by shearing, is shown by open arrows.

variable $q_i = \pm 1$ which is positive where the vacuum flux is upward or rightward and negative otherwise (fig. 2) the general change can be written

$$\dot{\Phi}_i^{(\mathrm{v})} \;=\; -\,q_i\,\dot{\phi} \quad . \tag{12}$$

The magnitude of flux change, $\dot{\phi}$, depends on the rate of shear and is the same for each separator.

The translational symmetry of the grid will result in a corresponding symmetry in the matrix M_{ij}. The symmetric definition of q_i then means that

$$\sum_j M_{ij}\,q_j \;=\; \mu\,q_i \quad , \tag{13}$$

where μ is a constant characterizing the grid. It can be shown that $\mu > 0$ in order to assure that the total magnetic energy is positive.

During the stressing phase all separators are in their normal states and $\dot{\Phi}_i = 0$. Using this in expression (8) along with (12) and (13)

$$\dot{I}_i \;=\; -\sum_j [M^{-1}]_{ij}\dot{\Phi}_j^{(\mathrm{v})} \;=\; q_i\,\dot{I} \quad , \tag{14}$$

where $\dot{I} = \dot{\phi}/\mu$. Thus the quantity q_i defines the sense of current change introduced by shearing, as shown in fig. 2.

The stressing phase begins with each current at I_i^n, and ends when the first one reaches its threshold. The first current will reach its threshold after

$$\Delta t_n \;\equiv\; \min_i |1 - q_i I_i^n| \quad , \tag{15}$$

where time has been rescaled to $I^\star/\dot{I}$. The stressing ends at this point with currents in their pre-reconnection state

$$I_i^{(n+1),0} \;\equiv\; I_i^n \;+\; q_i\,\Delta t_n \quad , \tag{16}$$

which has magnitude less than unity everywhere except where expression (15) achieves its minimum.

In general expression (15) will achieve a minimum at a single separator $i = \sigma$. This causes a reconnection episode during which $I_\sigma \to 0$. The current at each neighbor i changes according to the update vector U_i^σ, defined below. The complete set of changes constitute the first *generation* of the reconnection phase

$$I_i^{n,0} \to I_i^{n,1} \;=\; I_i^{n,0} \;+\; \Delta I_\sigma\, U_i^\sigma \quad . \tag{17}$$

The reconnection episode means $I_\sigma^{n,1} = 0$ so that $\Delta I_\sigma = -I_\sigma^{n,0}$ and $U_\sigma^\sigma = 1$. Other elements in the vector U_i^σ are calculated below.

The energy released by this episode is given by expression (11) where the value of $\mathcal{L}^{(\mathrm{eff})}$ (identical for all separators) will be found below. Rescaling energy to ΔE, each relaxation episode will liberate a single energy unit.

If all of the new currents remain below threshold, $|I_i^{n,1}| < 1$, then the reconnection phase ends after a single generation. Otherwise a second generation of reconnection episodes relaxes each of the offending currents. A general reconnection generation g consists of episodes at each of the separators σ where $|I_\sigma^{n,(g-1)}| \geq 1$. The current changes from each episode of a single generation are added together

$$I_i^{n,(g-1)} \to I_i^{n,g} \;=\; I_i^{n,(g-1)} \;+\; \sum_\sigma \Delta I_\sigma\, U_i^\sigma \quad , \tag{18}$$

so the order of relaxation within a generation is irrelevant. All relaxations reduce the excess current by unit magnitude, $\Delta I_\sigma = \pm 1$ with the sign opposite $I_\sigma^{n,(g-1)}$.

Once $|I_i^{n,g}| < 1$ for all separators i the reconnection phase of step n ends and step $n+1$ begins

$$I_i^n \overbrace{\rightarrow I_i^{n,0}}^{\text{stressing}} \underbrace{\rightarrow I_i^{n,1} \rightarrow I_i^{n,2} \rightarrow \cdots \rightarrow I_i^{n,g}}_{\text{reconnection}} = I_i^{n+1} \quad . \tag{19}$$

The stressing phase is given by eq. (16) and each reconnection generation by eq. (18). The complete reconnection phase describes a single flare shown schematically in fig. 3. The number of generations is the *duration* of the flare D_n. Since photospheric motions are slow compared to coronal Alfvén speeds flare durations are always shorter than the waiting times, although the two time scales are never directly compared in this model. Flare n is also characterized by its energy release E_n which, in units of ΔE, is the total number of relaxation episodes, and its peak rate P_n, which is the number of episodes in the largest generation.

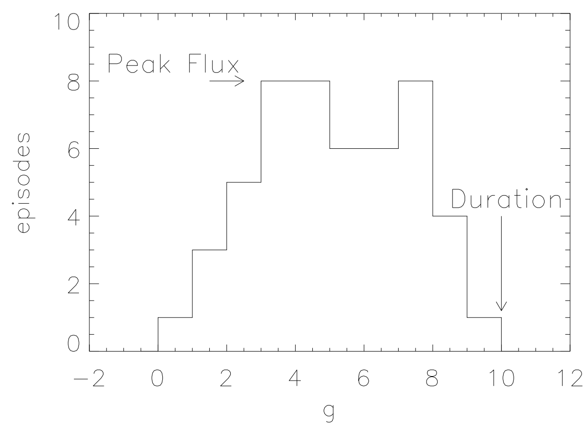

Fig. 3.—. The time history of a single flare of $D_n = 10$ generations with size $E_n = 50$ and peak $P_n = 8$.

3.1. The reconnection update vector

A reconnection episode at separator σ changes currents in neighboring elements by $\Delta I_i = \Delta I_\sigma\, U_i^\sigma$. During this episode separator σ is in the reconnective state so Φ_σ will change by some amount $\Delta\Phi_\sigma$. All other separators are in the normal state so $\Delta\Phi_i = 0$ for $i \neq \sigma$. These flux changes are summarized

$$\Delta\Phi_i \;=\; \sum_j M_{ij}\Delta I_j \;=\; \Delta\Phi_\sigma\,\delta_{i\sigma} \quad , \tag{20}$$

where $\delta_{i\sigma}$ is the Kronecker-δ. Solving this for the current changes

$$\Delta I_i \;=\; \Delta\Phi_\sigma \, [M^{-1}]_{i\sigma} \quad . \tag{21}$$

The $i = \sigma$ component provides the value of the effective self-inductance

$$\mathcal{L}^{(\mathrm{eff})} \;\equiv\; \frac{\Delta\Phi_\sigma}{\Delta I_\sigma} \;=\; \frac{1}{[M^{-1}]_{\sigma\sigma}} \quad , \tag{22}$$

accounting for the effect on Φ_σ of all changes in neighboring currents. Using this relationship the update vector can be concisely written

$$U_i^\sigma \;=\; \frac{[M^{-1}]_{i\sigma}}{[M^{-1}]_{\sigma\sigma}} \quad . \tag{23}$$

It is clear from this expression that $U_\sigma^\sigma = 1$, as predicted above.

In the spirit of a CA model we would like a single reconnection episode to be relatively local. Toward this end we will consider a mutual inductance matrix which couples a separator σ to only those neighbors with flux having a common source (see fig. 4). The seven non-vanishing elements in row σ of this reduced mutual inductance matrix are

$$\begin{array}{rccccccc} i = & \sigma & 1 & 2 & 3 & 4 & 5 & 6 \\ M_{\sigma i} \;=\; & \Big(\mathcal{L} & m_\perp & m_\parallel & -m_\perp & m_\perp & m_\parallel & -m_\perp \Big) \end{array} \tag{24}$$

where 1–6 refer to relative separator indices shown in fig. 4. The coefficients $m_\perp$ and $m_\parallel$ are mutual inductances between separators meeting at a corner or facing each other across a cell. For concreteness we will model each separator as a semi-circular wire, making $m_\perp$ and $m_\parallel$ one half-the mutual inductance between two circular wires of diameter L whose axes are perpendicular and parallel and whose centers are separated by $\sqrt{2}L$ and L respectively. The arithmetic sign of coefficient i shows the direction of flux induced at σ by a positive current at separator i.

Rescaling the inductance matrix to $m_\perp$,

$$\begin{aligned} M'_{\sigma i} \;&=\; (\;\; \mathcal{L}/m_\perp \quad 1 \quad m_\parallel/m_\perp \quad -1 \quad 1 \quad m_\parallel/m_\perp \quad -1 \;\;) \\ &=\; (\;\;\;\; f \qquad 1 \qquad a \qquad -1 \quad 1 \qquad a \qquad -1 \;\;) \end{aligned} \tag{25}$$

will not affect the update vector which depends on a ratio of elements from M^{-1}. The ratio of mutual inductances $a \equiv m_\parallel/m_\perp \simeq 0.12$ can be found (numerically) from the classic Neumann formula (Jackson 1975).

The rescaled self-inductance $f \equiv \mathcal{L}/m_\perp$ cannot be found so simply since the self-inductance of a separator current ribbon depends on the local field around

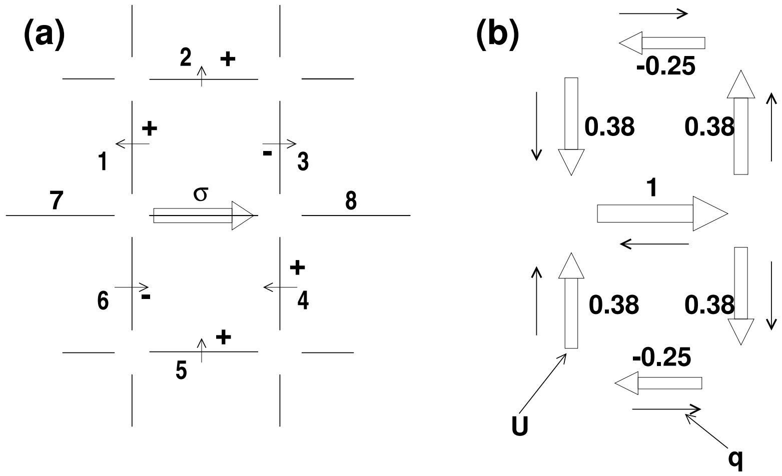

Fig. 4.—. The neighborhood of a horizontal separator. (a) The separator σ is inductively coupled to neighbors 1, 2, … 6. It is not coupled to 7 or 8 since these do not link flux from any sources common to σ. (b) The orientation of the currents for U_i^σ are shown in white along with their numerical values. The senses of q_i are shown in black.

the separator as well as the current it carries (Longcope & Cowley 1996). An exact application of the MCC to a separator network actually involves a system of coupled nonlinear equations (Longcope & Silva 1998). The nonlinearity derives from a self-inductance which depends on current logarithmically. We have chosen to approximate this as a constant, $\mathcal{L}$, which should be chosen to best approximate this nonlinear function over the full range of currents $0 \leq |I| \leq I^\star$. Since the threshold current $I^\star$ is a free parameter of the MCC model, the ratio f will also be a free parameter. In principal f is the only free parameter in our CA model, however, we show below that only one specific choice, $f = f_*$, results in a self-organized critical state.

Restricting the mutual inductive coupling to the nearest neighbors the matrix M contains six off-diagonal bands. This does not mean, however, that most elements of M^{-1} are non-zero. In order to localize the update vector U_i^σ we take the further step of inverting only the 7×7 matrix connecting σ and its neighbors

$$\tilde{M} = \begin{bmatrix} f & 1 & a & -1 & 1 & a & -1 \\ 1 & f & -1 & a & 0 & 0 & 0 \\ a & -1 & f & 1 & 0 & 0 & 0 \\ -1 & a & 1 & f & 0 & 0 & 0 \\ 1 & 0 & 0 & 0 & f & -1 & a \\ a & 0 & 0 & 0 & -1 & f & 1 \\ -1 & 0 & 0 & 0 & a & 1 & f \end{bmatrix} . \tag{26}$$

The two 3×3 blocks of zeros arise because neighbors 1–3 in the upper cell don't interact with 4–6 in the lower cell. Our CA model uses the update vector

$$U_i^\sigma = \frac{[\tilde{M}^{-1}]_{i\sigma}}{[\tilde{M}^{-1}]_{\sigma\sigma}} \quad . \tag{27}$$

Figure 5a shows the two distinct values of the update vector U_2^σ and U_3^σ, as a function of f. The signs of all components are shown graphically in fig. 4b. For extremely large self-inductance, $f \gg 1$, relaxation has little effect on neighbors, as indicated by $|U_i^\sigma| \ll 1$.

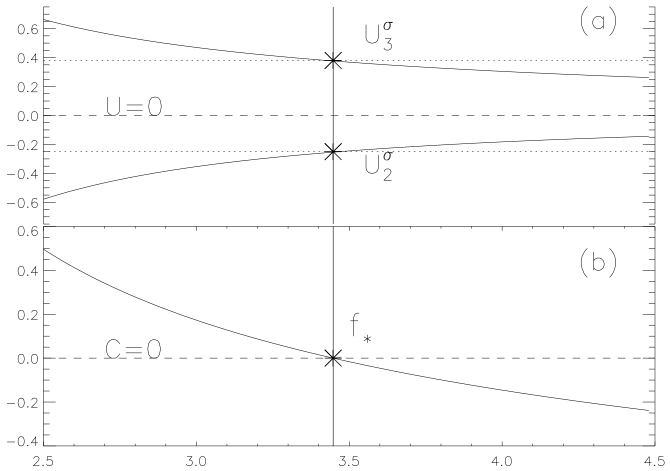

Fig. 5.—. The effect of the parameter f on the update vector U_i^σ. (a) The parallel and perpendicular components U_2^σ and U_3^σ respectively. (b) The function $C(f)$, defined in (28), which describes the change in total current from a single reconnection episode. The critical value $f_* \simeq 3.4475$ where $C(f) = 0$ is indicated, along with the values of $U_2^\sigma(f_*)$ and $U_3^\sigma(f_*)$.

When the separator σ is in the interior of the $N \times N$ grid all six neighbors will be updated according to the vector U_i^σ above. At an edge or a corner, however, σ will have fewer neighbors. We will ignore edge-effects upon the mutual inductance matrix and update the existing neighbors according to the appropriate elements of U_i^σ from eq. (27). For large grids only a fraction $\sim 4/N$ of the elements lie along the edge, so we would expect the approximation to be a good one..

3.2. Choosing the parameter f

The stressing phase "increases" each of the currents in the network according to eq. (16). The term "increase", as we use it here, means to change the current I_i in the q_i direction, which may be positive or negative. The first episode in the relaxation phase decreases that current I_σ which had exceeded its threshold. The six neighboring currents are either increased or decreased depending on the sign of U_i^σ relative to q_i. Consider the case where $q_\sigma = -1$ so $\Delta I_\sigma = +1$ as illustrated in fig. 4b. In this case eq. (18) dictates that each current is changed by U_i^σ. As shown in fig. 4b, the four perpendicular neighbors are increased while the two parallel neighbors are decreased.

It is important to determine whether a single relaxation episode results in an increase or decrease in currents overall. As the CA model reaches a statistical steady state the stressing phase will always increase the currents. If the average waiting time is $\langle \Delta t \rangle$ then the average total increase will be $2N^2\langle \Delta t \rangle$ in each stressing phase[1]. The current change during the relaxation phase will depend on the current change from a single relaxation episode. The total current change from a single relaxation episode in the grid interior is given by

$$C(f) \;=\; -\,q_\sigma \sum_i q_i U_i^\sigma \quad , \tag{28}$$

where the sum over i includes $i = \sigma$ as well as all six neighbors. This expression adds the increases, where U_i^σ and q_i have the same sign, and subtracts the decreases, where they have opposite signs. The function $C(f)$ is plotted in fig. 5b.

If $C(f) < 0$ then the single relaxation episode has decreased currents in σ and its parallel neighbors more than it has increased the currents in the perpendicular neighbors so the overall current has decreased. Since perpendicular neighbors are increased, sympathetic relaxations are possible in spite of the decreased overall current. The perpendicular neighbors will be driven past the threshold in the same direction they were stressed, q_i, so each subsequent episode will decrease the overall current by $-C(f)$. A complete reconnection phase of size E_n will decrease the total current by $-E_nC(f)$ (a positive number). This argument neglects the possibility of several neighboring flares driving a current I_i across the threshold in the direction opposite to q_i. We find that this seldom occurs and therefore does not affect our calculation.

Once in statistical steady state the reconnection phase must decrease the current, on average, by the same amount that the stressing phase increased it. Ignoring the effects of the edges, this implies that the average size of a flare is

$$\langle E_n \rangle \;=\; -\,\frac{2N^2\langle \Delta t \rangle}{C(f)} \quad , \tag{29}$$

---

[1]The factor of 2 arises because there are N^2 horizontal and N^2 vertical separators

which is positive since $C(f) < 0$.

Had the update vector created a net *increase* in current overall, $C(f) > 0$, there would be no hope of statistical steady state. Both stressing and reconnection would increase the current; nothing would decrease it. Eventually a single reconnection phase would feed off its own current increase, and never cease.

A critical state is that statistical steady state where the average size of a relaxation $\langle E_n \rangle$ diverges, at least in the limit of an infinite grid, $N \to \infty$. From expression (29) we see that this requires $C(f) = 0$. The particular value of the f which satisfies this is

$$f_* \simeq 3.4475 \quad , \tag{30}$$

as indicated in fig. 5b. Only with this value of the parameter f does a relaxation episode have the potential to propagate to arbitrary distances. We will choose $f = f_*$ for our model, making the update vector

$$U_i^\sigma = [1, -0.38, -0.25, 0.38, -0.38, -0.25, 0.38] \quad , \tag{31}$$

as shown in fig. 4b. The effective self-inductance is $\mathcal{L}^{(\mathrm{eff})} = 0.53 m_\perp$, which determines the scaling of the flare energies.

4. Results of the model

The CA model is run by first randomly initializing currents I_i. The initialization is the only random element in the model, since the iteration rules (16) and (18) are deterministic. The critical state should not depend on the details of initialization so we initialize the currents with normal deviates.

The CA is then iterated until it achieves a statistical steady state. A global quantity, such as the total unsigned current in the grid, will asymptotically approach its steady state value during this transient period. After statistical steady state is achieved (this typically takes 500 iterations) the model is iterated $\mathcal{N}$ times to accumulate flaring statistics. The waiting time Δt_n, duration D_n, peak P_n and energy E_n are recorded for each of the $\mathcal{N}$ flares. Histograms can be used to estimate the probability distribution of each variable.

Figure 6 shows the distributions of each variable, along with fits, from a run of $\mathcal{N} = 5,000$ iterations on a 30×30 grid. The χ^2 fitting is done over a restricted range of the distributed variable. For example, the flare energy distribution is modeled with the power-law

$$\frac{dp}{dE} \;=\; A_E \, E^{-\alpha_E} \quad , \tag{32}$$

over the range $10 \leq E_n \leq 1000$. The 3-σ error bars at each point reflect Poisson statistics in the bin. These error bars are then used to calculate the error in each of the fit parameters and the χ^2 goodness-of-fit. In all cases the χ^2 analysis indicates consistency with the model. The fitted powers for E, P and D are given in Table 1 along with errors and the median value for each quantity

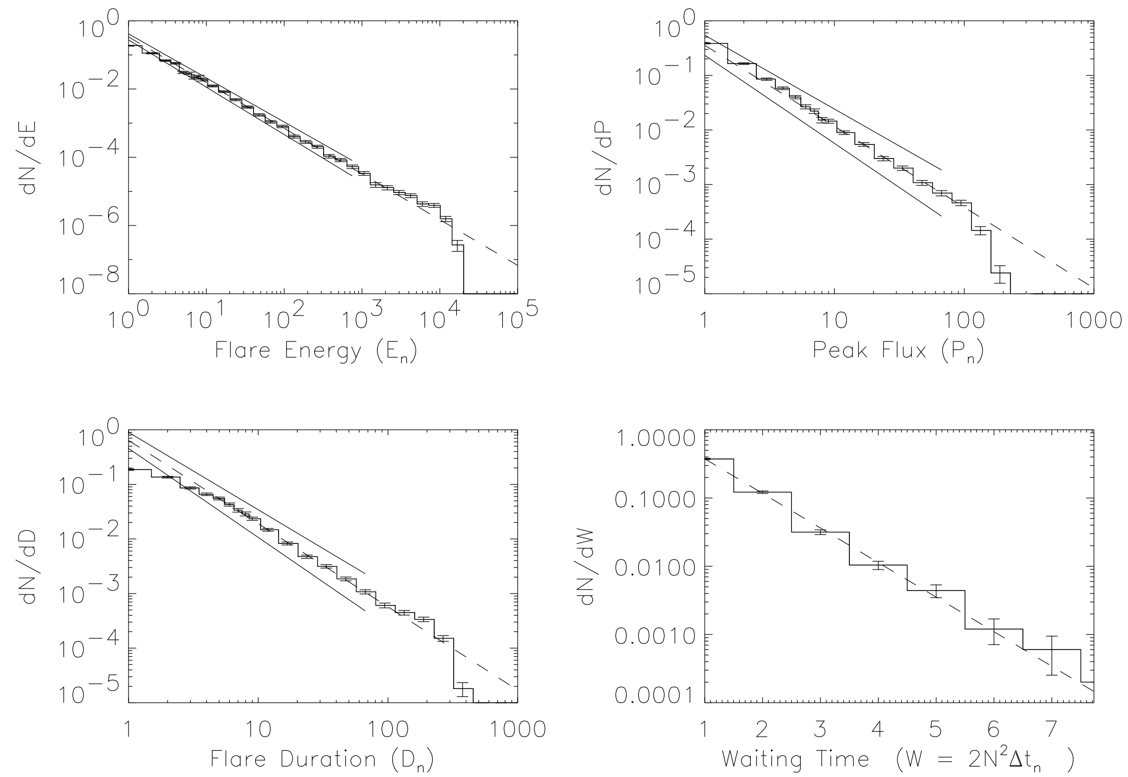

Fig. 6.—. Probability distributions calculated from histograms of $\mathcal{N} = 5,000$ flares on a 30×30 grid. (a) Flare energies E_n, (b) peak flux P_n and (c) flare duration D_n, each fit to a power-law. (d) Waiting time per element $2N^2\Delta t_n$, fit to an exponential.

The energy distribution follows a power-law until $E_n \simeq 3 \times 10^3$, where it rises slightly and rolls over. On a 30×30 grid a flare of an energy $E_n \simeq 3 \times 10^3$ must relax every one of the 1800 elements more than three times. Clearly the edges of the grid are not irrelevant in such a process. Performing runs on grids of varying sizes N shows that the roll-off location varies with grid size. Figure 7a compares the energy distributions from 30×30 and 300×300 grids, showing roll-off at $E_n = 3 \times 10^3$ and

$E_n = 3 \times 10^6$ respectively. Since the power-law exponent, $\alpha_E < 2$, the average energy is determined by the value of this roll-off.

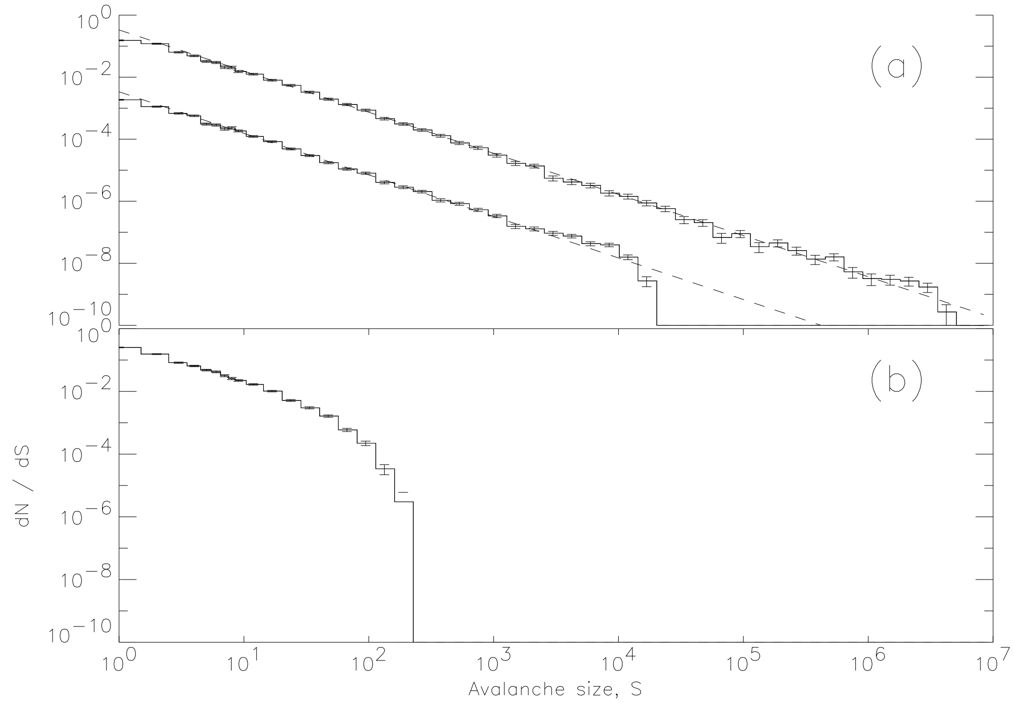

Fig. 7.—. Comparisons of energy distributions for different parameter choices. (a) A 30×30 grid (below) compared to a 300×300 grid (above). The lower curve shows $0.01 \times dp/dE$ for clarity. (b) A sub-critical model, $f = 3.8 > f_*$.

Neither the powers α nor the medians are affected by the grid size, but the averages, such as $\langle E \rangle$, are. Runs on still other grids yield a scaling

$$\langle E \rangle \simeq 0.6\, N^{1.9} \quad . \tag{33}$$

Thus in the limit $N \to \infty$ the average flare size diverges in accordance with the discussion above. This divergence is a natural consequence of a power-law with exponent less than two.

Choosing sub-critical values of the self-inductance, $f > f_*$, gives an energy distribution which falls off faster than any power-law (see fig. 7b). This distribution

	α	median
E	1.34 ± 0.05	7
P	1.48 ± 0.13	2
D	1.53 ± 0.11	5

Table 1:. Power-law exponents and median values for size-related quantities in the MCC/CA model.

has a finite $\langle E_n \rangle$ independent of N, as discussed above. Choosing a super-critical value, $f < f_*$, results in a reconnection phase which never ends, making statistical analysis impossible.

The exponential distribution of waiting times, fig. 6d, suggest that flares occur as a Poisson process. Recall that the iteration scheme itself is deterministic, so this is not a trivial result. More significantly, the waiting time Δt_n is only weakly correlated with any aspect of the subsequent flare's size, as typified by fig.8d. A long wait is not always rewarded by a large flare.

The three indicators of flare size, E_n, P_n and D_n, are all correlated with one another. Figure 8 shows scatter plots from the same $\mathcal{N} = 5,000$ flares shown in fig. 6. The power-law distributions predict the interrelations between the variables. The cumulative probability of a variable X

$$p(X) = \left(\frac{X}{X_0}\right)^{(1-\alpha_X)} \quad , \quad X \geq X_0 \ , \tag{34}$$

is the probability that $X_n > X$ in a given flare. If two variables, such as E_n and P_n were perfectly correlated then their cumulative probabilities would be equal leading to the relationship

$$P \ = \ P_0 \left(\frac{E}{E_0}\right)^{(1-\alpha_E)/(1-\alpha_P)} \quad . \tag{35}$$

The predicted relationships, shown in fig. 8, are reasonable but only approximate, perhaps owing to their inaccurate assumption that e.g. E_n and P_n are perfectly correlated.

5. Application to the solar corona

One of the primary advantages of the MCC/CA over previous work is that it has direct connection to MHD and coronal magnetic fields. The model's flux elements, Φ_0, represent the 10^{18} Mx flux tubes which appear to compose AR flux except in a sunspot (Zwaan 1987). A modest active region (AR) with $\Phi_{\rm AR} = 10^{22}$ Mx of unsigned flux consists of

$$N^2 = \frac{\Phi_{\rm AR}}{\Phi_0} = 10^4 \ \ . \tag{36}$$

such elemental tubes. To achieve an average field strength of $B_{\rm AR} = 100$ G, these elements must be distributed with a density of

$$n = \frac{B_{\rm AR}}{\Phi_0} = 1\,{\rm Mm}^{-2} \ . \tag{37}$$

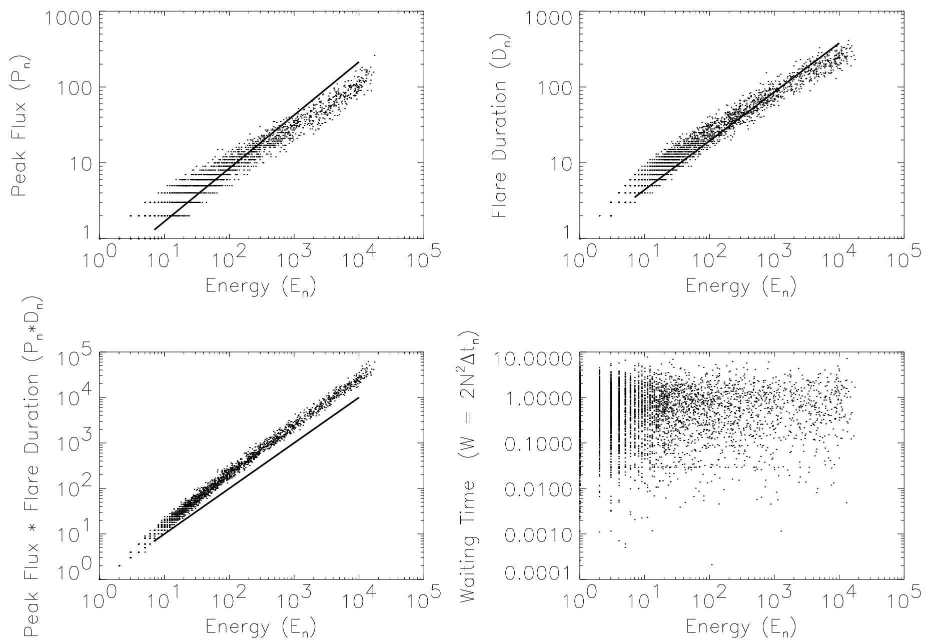

Fig. 8.—. Scatter plots of the $\mathcal{N} = 5,000$ flares from fig. 6. (a) Peak flux versus energy. (b) Duration versus energy. (c) The produce $P_n D_n$ versus energy. (d) Waiting time versus energy.

This could be modeled as a 100×100 grid whose spacing is $L = n^{-1/2} = 1$ Mm (i.e. an AR 100 Mm across).

Previous MCC investigations have found reconnection thresholds typically $I^\star \simeq 0.1\Phi^{(\mathrm{v})}/L \simeq 0.025\,\Phi_0/L$ (Longcope & Silva 1998) meaning that complete reconnection between two poles occurs in ~ 10 episodes. This threshold defines the basic unit of flare energy to be

$$E_0 \;\simeq\; 10^{-3}\,\Phi_0^2/L \;=\; 10^{25}\left(\frac{\Phi_0}{10^{18}\,\mathrm{Mx}}\right)^{3/2}\left(\frac{B_{\mathrm{AR}}}{100\,\mathrm{G}}\right)^{1/2}\mathrm{erg}\quad, \tag{38}$$

an order of magnitude larger than a "nanoflare" (Parker 1988). The median flare energy is $E_{\mathrm{med}} = 7E_0 \sim 10^{26}$ ergs regardless of AR size. The maximum flare energy $E_{\mathrm{max}} \simeq 3\times 10^5\,E_0 = 3\times 10^{30}$ ergs, is defined by the power-law's roll-off which depends on AR area. Indeed, there is observational evidence for this relationship between the AR size and the location of its high-energy roll-off (Kucera et al. 1997). Since the exponent $\alpha_{_E} < 2$, the roll-off also determines the average flare energy

$$\langle E\rangle \simeq 4\times 10^{28}\left(\frac{\Phi_{\mathrm{AR}}}{10^{22}\,\mathrm{Mx}}\right)^{0.95}\left(\frac{\Phi_0}{10^{18}\,\mathrm{Mx}}\right)^{0.55}\left(\frac{B_{\mathrm{AR}}}{100\,\mathrm{G}}\right)^{0.5}\mathrm{erg} \tag{39}$$

where the empirical scaling law for the MCC/CA eq. (33) has been used.

Flare waiting times will depend on the rate of stressing $\dot{I}$. An upper bound on these will come from the slowest source of photospheric motion which is differential rotation. Shearing at heliographic latitude λ (Howard, Gilman, & Gilman 1984) is

$$\frac{\partial v_x}{\partial y} = \omega = 6\times 10^{-7}\,\sin(2\lambda)\,\mathrm{rad/sec} \quad .$$

The vacuum flux, $\Phi^{(\mathrm{v})} = 0.25\Phi_0$, will change so that a given vertical pair completely decouples in time $1/\omega$, the time taken to separate by a horizontal distance L. This means that $\dot{\phi} = 0.25\,\omega\Phi_0$ and $\dot{I} = \dot{\phi}/\mu \simeq 0.01\,\omega\Phi_0/L$, since $\mu = 7.21 m_{\perp} \simeq 20L$. The unit of time is therefore

$$t_0 \equiv \frac{I^\star}{\dot{I}} = \omega^{-1} = \frac{2\times 10^6\,\mathrm{sec}}{\sin(2\lambda)} \quad ,$$

which is 6×10^6 sec at 15° latitude. This number is much larger than the Alfvén transit time, thereby justifying our instantaneous reconnection assumption. The mean waiting time between reconnection episodes,

$$\langle \Delta t\rangle \;=\; 0.83\,\frac{t_0}{2N^2} \;\simeq\; \frac{1.4\times 10^6\,\Phi_0}{\sin(2\lambda)\Phi_{\mathrm{AR}}} \quad , \tag{40}$$

is approximately 300 seconds in our example.

The average waiting time $\langle\Delta t\rangle$ is the interval between any two subsequent reconnection events, regardless of their size. Flares larger than an energy E comprise a fraction

$$p(E) = \left(\frac{E}{E_0}\right)^{1-\alpha_E} \quad , \tag{41}$$

of all events as given in eq. (34). The waiting time between these larger flares is then longer than the mean waiting time by a factor $1/p(E)$. Thus, flares larger than $E = 10^{29}$ ergs recur with a mean waiting time of 6000 seconds (2 hours) in a 10^{22} Mx AR at 15° latitude. On the other hand, for the exponent $\alpha_E = 1.6$ found from observations the mean waiting time would be ten times longer: 6×10^4 seconds (1 day).

The actual interval between flares of GOES C-class or greater was approximately 1.7×10^4 sec (5 hours) in 1999 (1815 GOES flares were recorded that year). The average number of NOAA active regions on the disk in 1999 was 7.4, making the mean interval in any single AR 1.3×10^5 sec (36 hours), slightly longer than the MCC/CA value.

Since flare energy and mean heating rate are almost uncorrelated we can divide them to yield the average power from flaring in a single AR

$$\bar{\mathcal{P}} \;=\; 2\times 10^{26}\,\sin(2\lambda)\left(\frac{\Phi_{\rm AR}}{10^{22}\,{\rm Mx}}\right)^{1.95}\left(\frac{\Phi_0}{10^{18}\,{\rm Mx}}\right)^{-0.45}\left(\frac{B_{\rm AR}}{100\,{\rm G}}\right)^{0.5}{\rm erg\,sec}^{-1}\quad . \qquad (42)$$

This is an order of magnitude larger than the power in observed flares found by Hudson (1991). Dividing $\bar{\mathcal{P}}$ by the AR area, $\Phi_{\rm AR}/B_{\rm AR} = 10^{20}\,{\rm cm}^2$ yields a heat flux of $F \simeq 2\times 10^6\,{\rm erg\,sec}^{-1}\,{\rm cm}^{-2}$, too small to sustain an AR corona (Withbroe & Noyes 1977). A similar deficit is found from direct calculation of the power in observed flare frequency distributions (Hudson 1991, Shimizu 1995). In this respect the observational and theoretical results agree: flares and microflares do not dissipate sufficient energy to maintain the corona's energy budget. One explanation proposed for the observed deficit is that a population of "nanoflares" are distributed with an exponent $\alpha_{_E} > 2$ and supply the remaining power. Evidence for such a population remains controversial (Krucker & Benz 1998, Parnell & Jupp 2000).

Fisher *et al.* (1998) calculated magnetic fluxes and X-ray luminosities for 333 ARs between 1991 and 1995. They found that 10^{22} Mx ARs had a median X-ray luminosity of $L_x \simeq 1.2\times 10^{26}\,{\rm erg\,sec}^{-1}$, comparable to (42). Their study also found that the luminosity scaled as $\Phi_{\rm AR}^{1.19}$ rather than $\Phi_{\rm AR}^{1.95}$. Quadratic scaling with $\Phi_{\rm AR}$, as in eq. (42), is a characteristic of quasi-static calculations like MCC (Longcope 1998, Fisher et al. 1998). Fisher *et al.* proposed a reconciliation of these facts by postulating that ARs are "self-similar" and thus that $N^2 \sim \Phi_{\rm AR}/\Phi_0$ was a constant.

6. Discussion

The foregoing has presented a new cellular automaton model for solar flares. The model's rules are derived from an approximation of the minimum current corona (MCC) model, which is itself an approximation of MHD. This new model, called the MCC/CA, demonstrates a natural manner by which magnetic reconnection in a complex magnetic field may be described by theories of self-organized criticality. This opens the possibility that solar flares obey a power-law frequency distribution because each flare is the product of many small reconnection episodes.

6.1. Effects of the approximations

The significance of this result should be examined in light of the two significant layers of approximation in the derivation of the model. First the dyanmical equations of MHD are approximated by the quasi-static theory of MCC. Second, the MCC is applied to a simplified arrangement of sources (a square lattice), and then approximated as a set of CA rules. Possible effects of each approximation are considered below. In the end, however, CA models are not typically proposed as calculational tools, but are intended to model the way that a collection of interacting components behaves. Each approximation must be judged according to its possible effects on this modest objective.

The minimum current corona model follows from MHD after several approximations. First it assumes an ideal, high-β corona in the quasi-static limit. Under this assumption the magnetic field will remain in its state of minimum energy at all times. It further assumes the entire field arises from isolated photospheric sources which lack the detailed internal structure necessary to tie individual field lines. This leaves a countable set of constraints on the magnetic energy minimization, namely the total flux linking any pair of opposite charges. Subject to only these constraints, the general state of minimum energy state will be current-free except for possible current sheets at the interfaces of the constained fluxes (i.e. the separators, Longcope and Cowley 1996).

Barring reconnection separator currents would build up indefinitely, in obvious condradiction to the observed solar corona. Stick-slip reconnection is introduced to resolve this final contradiction, and create a model with properties similar to those of the real solar corona. The validity of all three assumptions of the MCC is a topic of several past investigations (Longcope & Silva 1998, Longcope & Kankelborg 1999, Kankelborg & Longcope 2000) with still more underway. It is too early yet to assess the calculational accuracy of this approximation.

In a sufficiently complex coronal field, the minimum current corona model contains those basic ingredients usually invoked for self-organized criticality (Lu 1995). Namely, there are many discrete elements (separators) which individually store and relieve stress, and can interact with one another. It may eventually be possible to show that the field from any large but abribtrary collection of photospheric sources will exhibit SOC in its reconnection. Doing so would require a method of deriving properties of the network of separators which arise from an arbitrary collection of sources; this is not yet possible (Welsch & Longcope 1999). As an initial step we have analyzed the properties of a very specific network of sources: an alternating square lattice.

The distribution of magnetic sources in a real active region differs from our lattice model in numerous respects. Perhaps the best way to test the effects of these differences will be to modify, in future work, the existing CA rules to more accurately approximate observed magnetic field properties. In the meantime it is posible to anticipate which of these modifications might effect the fundamental result of SOC, and which may effect the power-law exponent.

An actual active region consists of positive and negative flux elements with a range of fluxes, rather than the uniform flux distribution of our model. More significantly, sources of one sign tend to remain spatially clustered, mixing with opposing sources mostly along the region's neutral line. Some sources therefore have few opposing neighbors with which to share flux while others have many. In future work it may be possible to investigate this effect using a square lattice by allowing non-uniform charges and relaxing the assumption of strict alternation. It seems unlikely that an inhomogeneous lattice, such as one with a neutral line, would exhibit self-organized criticality since criticality requires homogeneity and lack of natural scale. This same prediction can, however, be made of all SOC models and points to their most serious limitation.

Flux sources in an active region are not aligned on a reqular lattice, but are concentrated along the boundaries of super-granular cells. These cells form an irregular lattice known as a Voronoi teselation (Hagenaar, Schrijver, & Title 1997) whose properties differ from a square lattice in interesting ways. Further investigation can show how the choice of lattice pattern affects the CA model and its results.

It also remains to investigate the effects of one final layer of rather technical approximations made in defining the CA rules. Mutual inductance was limited to nearest-neighbors, to yield a managable matrix M. Next the update vector was calculated by approximating the inverse of M. Relaxing either assumption would simply result in different update vector U_i^σ, which changes current in more neighbors. Previous investigations have found that changing details of the CA rules has no affect on the self-organized criticality and little effect on the power-law exponents (Kadanoff et al. 1989). We mention below that we might expect changes to U_i^σ to effect the power-law exponent, but not to eliminate the SOC behavior.

The self-induactance f was the only free parameter in the derivation of the CA rules. We found that only the specific choice $f = f_* = 3.4475$ led to self-organized criticality. In a certian sense this renders the model "less self-organized" and more like an Ising model in which an external field (i.e. temperature) defines the critical state. It would be more satisfying if a mechanism existed by which the self-induactance of a current ribbon might naturally adjust itself to this critical value. At present we can offer no such mechanism.

6.2. The power-law exponents

The present work is intended as a first step down this road of investigating the properties of complex MCC models. It has established that self-organized criticality does result from magnetic reconnection in complex coronal magnetic fields. As an immediate consequence, we have found that reconnection events can span an arbitrary range of sizes, and are distributed according to a power-law. The exponent of this power-law, $\alpha_E = 1.34 \pm 0.05$, differs from that of observed flares at a statistically significant level. Since existing SOC models, such as LH, exhibited power-laws whose exponents agreed much more closely with observations, it would seem that the MCC/CA is a step backward. Such a conclusion is premature until those obvious modifications described above are shown to produce no better agreement. It should also be noted that the MCC/CA uses a more conventional MHD approach than the LH model does to derives its rules.

The MCC/CA exhibits an energy exponent, $\alpha_E = 1.34 \pm 0.05$, lower than the three-dimensional sandpile-based models, such as LH, for which $\alpha_E = 1.5$. Since it is a two-dimensional model, however, the MCC/CA might also be compared to two-dimensional sandpile models, which have the exponent is $\alpha_E = 1.05$. This discrepancy further emphasizes the difference between this and previous CA flare models. It has been observed that CA models with anisotropic rules belong to a different universality class, and thus show different exponents (Kadanoff et al. 1989, Vlahos et al. 1995). This may completely explain the difference, since the MCC/CA uses an update vector U_i^σ which is anisotropic, treating parallel and vertical neighbors differently. If this is the source of the discrepancy then it is possible that further modifications to the update vector will result in still different power-law exponents.

Finally, it is highly encouraging that the MCC/CA produces numerical predictions which are within reasonable range of observed physical values. The predicted flare energies, interval between flares, and total heating power, are all within an order of magnitude of those observed. Furthermore, their predicted scalings with $\Phi_{\rm AR}$ and $B_{\rm AR}$ are subject to future observational test. Several of these scalings are probably common to all SOC models, and might be a good basis for testing this general class of model. The values may change under any of the modifications to MCC/CA mentioned above, however, the basic scalings will probably not.

We wish to thank Dr. R. C. Canfield for help with some observational data.

This material is based upon work supported by the National Science Foundation under Grant No. ATM-9733424.

References

Bak, P., Tang, C., & Wiesenfeld, K. 1988, Phys. Rev. A, 38, 364

Bromund, K. R., McTiernan, J. M., & Kane, S. R. 1995, ApJ, 455, 733

Carlson, J. M., & Langer, J. S. 1989, Phys. Rev. Lett., 62, 2632

Chou, Y.-P. 1999, ApJ, 527, 958

Crosby, N. B., Aschwanden, M. J., & Dennis, B. R. 1993, Solar Phys., 143, 275

Dennis, B. R. 1985, Solar Phys., 100, 465

Fisher, G. H., Longcope, D. W., Metcalf, T. R., & Pevtsov, A. A. 1998, ApJ, 508, 885

Gold, T., & Hoyle, F. 1960, MNRAS, 120, 89

Greene, J. M. 1988, JGR, 93, 8583

Hagenaar, H. J., Schrijver, C. J., & Title, A. M. 1997, ApJ, 481, 988

Held, G. A., Solina, D. H., Keane, D. T., Haag, W. J., Horn, P. M., & Grinstein, G. 1990, Phys. Rev. Lett., 65, 1120

Howard, R. F., Gilman, P. A., & Gilman, P. I. 1984, ApJ, 283, 373

Hudson, H. S. 1991, Solar Phys., 133, 357

Jackson, J. D. 1975, Classical Electrodynamics (New York: Wiley)

Kadanoff, L. P., Nagal, S. R., Wu, L., & Zhou, S. 1989, Phys. Rev. A, 39, 6524

Kane, S. R., Hurley, K., McTiernan, J. M., Sommer, M., Boer, M., & Niel, M. 1995, ApJ, 446, L47

Kankelborg, C. C., & Longcope, D. W. 2000, Solar Phys., In press

Krucker, S., & Benz, A. O. 1998, ApJ, 501, L213

Kucera, T. A., Dennis, B. R., Schwartz, R. A., & Shaw, D. 1997, ApJ, 475, 338

Lau, Y.-T., & Finn, J. M. 1991, ApJ, 366, 577

Lin, R. P., Schwartz, R. A., & Kane, S. R. 1984, ApJ, 283, 421

Longcope, D. W. 1996, Solar Phys., 169, 91

Longcope, D. W. 1998, ApJ, 507, 433

Longcope, D. W., & Cowley, S. C. 1996, Phys. Plasmas, 3, 2885

Longcope, D. W., & Kankelborg, C. C. 1999, ApJ, 524, 483

Longcope, D. W., & Silva, A. V. R. 1998, Solar Phys., 179, 349

Lu, E. T. 1995, ApJ, 446, L109

Lu, E. T., & Hamilton, R. J. 1991, ApJ, 380, L89

Lu, E. T., Hamilton, R. J., McTiernan, J. M., & Bromund, K. R. 1993, ApJ, 412, 841

MacKinnon, A. L., & Macpherson, K. P. 1997, A&A, 326, 1228

Parker, E. N. 1988, ApJ, 330, 474

Parnell, C. E., & Jupp, P. E. 2000, ApJ, 529, 554

Shimizu, T. 1995, Publ. Astron. Soc. Japan, 47, 251

Sweet, P. A. 1958, Nuovo Cimento, 8, 188
Vassiliadis, D., Anastasiadis, A., Georgoulis, M., & Vlahos, L. 1998, ApJ, 509, L53
Vlahos, L., Georgoulis, M., Kluiving, R., & Paschos, P. 1995, A&A, 299, 897
Welsch, B. T., & Longcope, D. W. 1999, ApJ, submitted
Withbroe, G. L., & Noyes, R. W. 1977, ARA&A, 15, 363
Zirker, J. B., & Cleveland, F. M. 1993, Solar Phys., 145, 119
Zwaan, C. 1987, ARA&A, 25, 83

This preprint was prepared with the AAS LaTeX macros v4.0.